Available online at www.sciencedirect.com
SCIENCE DIRECT
ELSEVIER
Earth and Planetary Science Letters 240 (2005) 168–178
EPSL
www.elsevier.com/locate/epsl

Hematite spherules in basaltic tephra altered under aqueous, acid-sulfate conditions on Mauna Kea volcano, Hawaii: Possible clues for the occurrence of hematite-rich spherules in the Burns formation at Meridiani Planum, Mars

R.V. Morris [a,*], D.W. Ming [a], T.G. Graff [b], R.E. Arvidson [c], J.F. Bell III [d], S.W. Squyres [d], S.A. Mertzman [e], J.E. Gruener [a], D.C. Golden [f], L. Le [f], G.A. Robinson [f]

[a] *NASA Johnson Space Center, Houston, TX 77058, USA*
[b] *Arizona State University Tempe, AZ 85287, USA*
[c] *Washington University, St. Louis, MO 63130, USA*
[d] *Cornell University, Ithaca, NY 14853, USA*
[e] *Franklin and Marshall College, Lancaster, PA 17604, USA*
[f] *Jacobs Sverdrup Technologies, Houston, TX 77058, USA*

Accepted 22 September 2005
Available online 4 November 2005
Editor: A.N. Halliday

Abstract

Iron-rich spherules (>90% Fe_2O_3 from electron microprobe analyses) ~10–100 μm in diameter are found within sulfate-rich rocks formed by aqueous, acid-sulfate alteration of basaltic tephra on Mauna Kea volcano, Hawaii. Although some spherules are nearly pure Fe, most have two concentric compositional zones, with the core having a higher Fe/Al ratio than the rim. Oxide totals less than 100% (93–99%) suggest structural H_2O and/or OH^{-1}. The transmission Mössbauer spectrum of a spherule-rich separate is dominated by a hematite (α-Fe_2O_3) sextet whose peaks are skewed toward zero velocity. Skewing is consistent with Al^{3+} for Fe^{3+} substitution and structural H_2O and/or OH^{-1}. The grey color of the spherules implies specular hematite. Whole-rock powder X-ray diffraction spectra are dominated by peaks from smectite and the hydroxy sulfate mineral natroalunite as alteration products and plagioclase feldspar that was present in the precursor basaltic tephra. Whether spherule formation proceeded directly from basaltic material in one event (dissolution of basaltic material and precipitation of hematite spherules) or whether spherule formation required more than one event (formation of Fe-bearing sulfate rock and subsequent hydrolysis to hematite) is not currently constrained. By analogy, a formation pathway for the hematite spherules in sulfate-rich outcrops at Meridiani Planum on Mars (the Burns formation) is aqueous alteration of basaltic precursor material under acid-sulfate conditions. Although hydrothermal conditions are present on Mauna Kea, such conditions may not be required for spherule formation on Mars if the time interval for hydrolysis at lower temperatures is sufficiently long.

Keywords: Mars; Meridiani Planum; Mars Exploration Rover; Spherule; hematite; concretions; sulfate

* Corresponding author. Tel.: +1 281 483 5040; fax: +1 281 483 5173.
E-mail address: richard.v.morris@nasa.gov (R.V. Morris).

0012-821X/$ - see front matter © 2005 Elsevier B.V. All rights reserved.
doi:10.1016/j.epsl.2005.09.044

1. Introduction and background

The scientific basis for selection of Meridiani Planum as the landing site for the Mars Exploration Rover (MER) Opportunity centered on detection of the mineral hematite (α-Fe_2O_3) by the Thermal Emission Spectrometer instrument on the Mars Global Surveyor spacecraft [1–4]. High hematite concentrations are plausible though not definitive mineralogical markers for aqueous processes, making Meridiani Planum a viable location to land and attempt to study the products of aqueous processes in situ. Hematite was also detected in Aram Chaos and several isolated locations in Valles Marineris, but only the Meridiani Planum site was considered safe for landing [4].

The Miniature Thermal Emission Spectrometer (Mini-TES) and Mössbauer Spectrometer (MB) instruments on Opportunity confirmed the presence of hematite at Meridiani Planum. Specifically, Mini-TES detected hematite in an accumulation of spherical particles (spherules) on a sulfate-rich outcrop surface and in lag deposits elsewhere [5]. As shown by observations with the Panoramic Camera (Pancam) and Microscopic Imager (MI), the hematite-rich lag deposits correspond to spherules that were originally imbedded within outcrops and have weathered out from surrounding and softer sulfate-rich rock and accumulated as whole and broken spherules ~1–8 mm in diameter [6–10]. Spherules currently imbedded in the outcrop have a mean diameter of 4.2 ± 0.8 mm [11]. MB found high concentrations of hematite in sulfate-rich outcrops (the Burns formation), in the same accumulation of spherules analyzed by Mini-TES, and in ripple crest soils that are accumulations of whole and broken spherules (lag deposits) [12]. The high Hm concentration in deposits with broken spherules [12] and Pancam spectra of spherules sectioned by the MER Rock Abrasion Tool (RAT) [10] both show that hematite is present throughout the spherule volume and not just present as a coating.

Two populations of hematite are present in the outcrop, because MB spectra of outcrop rock for which the instrument's field of view was free of spherules show that ~40% of the Fe in the sulfate-rich rock is present as hematite [12]. Although analyses of spherule-rich targets by the Opportunity Alpha Particle X-ray Spectrometer (APXS) show high concentrations of total iron (>30% calculated as Fe_2O_3) and low concentrations of SiO_2 (<38%) [13], the nominal chemical composition of spherules is currently not known.

There is substantial evidence that the hematite-rich spherules in the Meridiani outcrop are concretions [10]. These concretions may have formed rapidly from breakdown of pre-existing jarosite or other iron sulfates during diagenesis when a "chemically distinct groundwater recharge event" occurred [11]. Formation of the spherules represented one of the latter phases of formation and alteration of the layered rocks encountered by Opportunity. The question addressed in this paper is whether or not there are mineralogical and elemental terrestrial analogues for these spherules whose formation pathways are consistent with formation by aqueous processes and that might provide insight into the overall system that produced the layered sulfate-rich deposits observed by Opportunity.

According to [14], diagenetic, hematite-cemented concretions found in the Jurassic Navajo Formation (quartz arenite in southern Utah) are possible terrestrial analogues for Meridiani spherules. The Navajo Formation (NF) concretions form in porous, relative insoluble quartz arenite by dissolution of iron oxides by reducing fluids and subsequent Fe precipitation to form spherical Fe- and Si-rich concretions ($SiO_2 > 60\%$) when the Fe-rich fluids encounter oxidizing groundwater [14]. Compared to Meridiani Planum (MP) spherules, however, NF spherules have a higher value for the SiO_2/Fe_2O_3 ratio (>1.5 and <1.3 and for NF and MP spherules, respectively) and are therefore not good compositional analogues for Meridiani spherules. However, the formation process for NF spherules may be broadly applicable to Meridiani Planum. Simplistically, the process would involve percolation of reducing, Fe^{2+}-rich, and perhaps sulfate-rich fluids through porous material with basaltic bulk composition and precipitation of Fe^{3+}-rich concretions when oxidizing conditions are encountered. An important consideration for this model applied to Meridiani Planum is whether fluid transport can be maintained in a material that is likely to be considerably more soluble with respect to the Fe^{2+}-rich fluid than quartz.

In this paper, we report a terrestrial mineralogical and morphological analogue for the Meridiani Hm- and Fe-rich spherules. The terrestrial spherules were formed in association with aqueous, acid-sulfate alteration of basaltic material on Mauna Kea volcano (Hawaii). The Mauna Kea (MK) spherules are mineralogically hematite and have $SiO_2/Fe_2O_3 < 0.04$.

2. Samples and methods

Sample HWMK745R is a clastic volcanic breccia rock (~10 cm in diameter) collected at ~13,000 ft on the Puu Poliahu cone of Mauna Kea volcano on the island of Hawaii. Puu Poliahu is a subaerial cinder cone that

has undergone pervasive acid-sulfate alteration to the sulfate mineral natroalunite ($(Na,K)Al_3(SO_4)_2(OH)_6$, with Na>K) and other phases when hot S-rich volcanic vapors and/or fluids percolated up through the cone [15]. From our traverses, we estimate the areal extent of the alteration zone is ~1 km^2, which is effectively the entire area occupied by the cone. The sulfate mineral jarosite ($(K,Na)Fe_3(SO_4)_2(OH)_6$), phyllosilicates, zeolites, and hematite have also been reported as alteration products on Puu Poliahu and on nearby cones in the summit region of Mauna Kea [15–19]. The K–Ar age for lava flows from Puu Poliahu is 53 ± 14 kA, and they have the hawaiite–mugearite composition that is typical of Laupahoehoe volcanic sequences [15].

As observed with a binocular microscope, the Mauna Kea breccia contains irregular, usually vesicular clasts of tephra (~1 mm to 2 cm in the longest dimension) dispersed in a cement that is white to yellow in color. Clasts are black to red in color. The breccia is heterogeneous in texture and contains areas that are predominantly the cementing material on the scale of 2 cm and areas that are predominantly clasts with narrow bands (1–4 mm) of cement between them. Black particles having diameters too small to be measured with a binocular microscope are heterogeneously distributed and embedded within certain areas of the cement with a high number density. Examination of a polished thick section in reflected light with a petrographic microscope showed that the black particles are highly reflective (oxides) and many are circular in cross section, implying a spherical shape. A concentrate (~5 mg) of spherules was obtained by grinding a spherule-rich portion of the breccia, dry sieving at 45 μm, forming an ethanol slurry, and using centrifugal force to separate the relatively high-density, low-albedo spherules from high-albedo cement and tephra fragments. A polished grain mount was prepared from a portion of the spherule separate.

Transmission Mössbauer spectra (293 K) were obtained on a 2.6 mg sample of the <45 μm separate of spherules and on a whole-rock powder (cement plus clasts). Whole-rock powders were also used for analysis by powder X-ray diffraction (XRD) and for measurement of major element compositions, Fe^{2+}/Fe^{3+}, and weight loss on ignition by X-ray fluorescence, titration for Fe^{2+}, and heating at 950 °C in air, respectively. Major elements were determined from the heated sample, so total Fe is reported as Fe_2O_3. Electron microprobe (EMP) analyses for major and minor elements and elemental maps were obtained from a polished grain mount of the spherules and a polished thick section of breccia that contained spherules. Scanning electron microscope (SEM) images were obtained on individual 500–1000 μm particles of breccia that contained spherules and surrounding medium and on individual whole and broken spherules; spherule were broken by gentle crushing with a mortar and pestle. Except for the EMP and SEM, instruments and analytical procedures are described by [19] and references therein. The EMP was a CAMECA 100SX, and it was operated at a beam voltage, current, and spot size of 15 kV, 20 nA, and 1.0 μm, respectively, for elemental analyses. For elemental maps, the beam was rastered in 0.2 μm steps, and the beam voltage, current, and spot size were 20 kV, 20 nA, and 1.0 μm, respectively. The SEM was a JEOL JSM 5910LV configured with a energy dispersive spectroscopy (EDS) system from IXRF Systems. Data were collected using a beam voltage 15 kV, and samples were mounted on a carbon substrate and carbon coated.

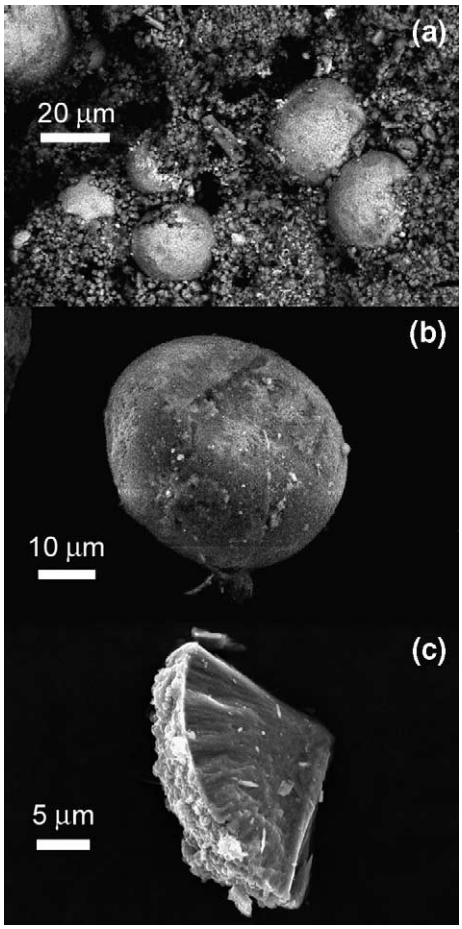

Fig. 1. Scanning electron microscope images of (a) spherules imbedded in breccia HWMK745R, (b) an individual spherule separated from the rock, and (c) a fragment of a broken spherule.

3. Results and discussion

3.1. Spherules

SEM photomicrographs of breccia particles with imbedded spherules, an individual spherule, and a broken spherule are shown in Fig. 1. The spherules are typically 10–100 μm in diameter and occur as single and intergrown spherules. The spherules typically fracture with the radial texture shown in Fig. 1c. Backscatter electron (BSE) images obtained from the spherule separate show that both single and intergrown spherules typically have two concentric zones (Fig. 2), although un-zoned spherules do occur. Regions of lower atomic number (Z) form a rim of roughly constant width around a core of higher Z material. Rim widths vary from spherule to spherule. The transition between zones is sharp, and the value of Z within each zone is relatively constant. The zones with different Z are observed when the polished grain mount containing the spherules is examined with a petrographic microscope using reflected light. Some spherules have void spaces and irregular-shaped regions of lower Z within the spherules (Fig. 2c).

EMP major element analyses of 16 spherules are summarized in Table 1. Total iron is calculated as Fe_2O_3. The spherule analysis totals are 93% to 99%, and we presume the deficit results from unknown pro-

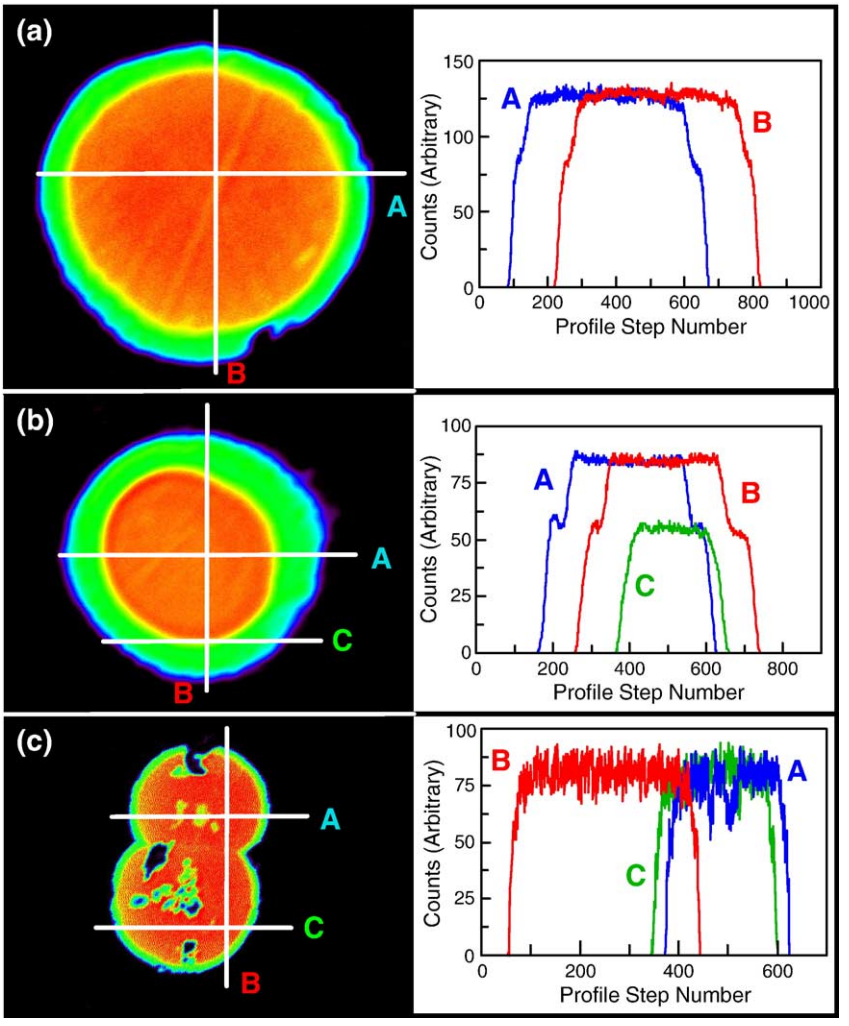

Fig. 2. False-color backscatter electron image of two individual hematite spherules and one doublet spherule. White lines correspond to locations of the horizontal and vertical profiles through the spherules that are shown to the right of each particle. Spherules in (a) and (b) have outer rims that have lower average atomic numbers (Z) than interior regions. In addition to a low-Z rim, the doublet spherule has interior voids and irregular shaped patches of low-Z material (c). Electron microprobe analyses show the low-Z regions have higher (Al+Si)/Fe ratio than high-Z regions. Note that the boundaries between regions of different values of Z are sharp.

Table 1
Core and rim electron microprobe analyses of spherules in breccia HWMK745R

	Core		Rim
	Average[a] (%)	Fe-rich[b] (%)	Average[c] (%)
SiO_2	1.93	0.72	2.82
TiO_2	0.02	0.03	0.03
Al_2O_3	2.81	0.57	6.95
Cr_2O_3	0.01	0.01	0.01
Fe_2O_3T	90.90	96.76	81.61
MnO	0.09	0.09	0.10
MgO	0.07	0.22	0.18
CaO	0.31	0.13	0.32
Na_2O	0.01	0.01	0.01
K_2O	0.02	0.01	0.02
P_2O_5	0.06	0.00	0.20
SO_3	0.32	0.12	0.46
CoO	0.00	0.00	0.00
NiO	0.02	0.04	0.01
Total	96.56	98.72	92.70

[a] 16 spherules.
[b] 2 spherules.
[c] 8 spherules.

portions of submicroscopic inclusions of H_2O and structural H_2O and/or OH^{-1}. The probable presence of structural H_2O/OH^{-1} is based on the work of [20] who conclude from various lines of evidence that hematite hydrothermally synthesized from Fe-sulfate solutions is described by the general formula $\alpha\text{-}Fe_{(2-x/3)}\square_{(x/3)}(OH)_xO_{(3-x)}\bullet nH_2O$ ($\square$ = cation vacancy). Upon heating in air, their hematite precipitate sample M60 lost H_2O by ~200 °C and structural OH^{-1} groups by ~900 °C. The hematite-like materials can be considered as solid solutions that are bounded by hydrohematite ($\alpha\text{-}Fe_{(2-x/3)}\square_{(x/3)}(OH)_xO_{(3-x)}$), protohematite ($\alpha\text{-}Fe_2O_3\bullet nH_2O$), and hematite ($\alpha\text{-}Fe_2O_3$) [20]. As expected from the BSE images, the cores of Mauna Kea spherules are enriched in Fe and depleted in Al and Si (average ~91% Fe_2O_3, ~3% Al_2O_3, and ~2% SiO_2) relative to their rims (average ~82% Fe_2O_3, ~7% Al_2O_3, and ~3% SiO_2). The two most Fe-rich spherules have cores with ~97% Fe_2O_3. Element maps of Si and Al (not shown) reproduce the same pattern as the BSE images (Fig. 2), so they are (within spatial detection limits) distributed homogeneously throughout the core and rim volumes.

The Mössbauer spectrum (293 K) of the spherule concentrate is characterized by a sextet whose individual peaks are skewed toward zero velocity and by a weak doublet (Fig. 3). The figure also shows Mössbauer spectra for whole-rock HWMK745R and a sample containing a mixture of synthetic and well-crystalline hematite (HMS3) and goethite (α-FeOOH; GTS5) [21]. The sextet and doublet characteristic of the spherule concentrate are present in the spectrum of the bulk breccia, except their relative intensities are reversed. Although the doublet in the spectrum of spherule concentrate could be intrinsic to the spherules, more likely it results from the non-spherule portion of the concentrate.

One conclusion is that the mineralogical composition of MK spherules is hematite. There is no indication for the presence of a goethite sextet in the Mössbauer spectrum of the spherules, so that the low totals for the elemental concentrations (Table 1) do not result from the presence of that phase. The presence of hematite is confirmed by fitting the peaks to asymmetric Lorentzian lineshapes and calculating the isomer shift (δ), quadrupole splitting (ΔE_Q), and hyperfine field strength (B_{hf}) from the derived peak positions (Table 2). These

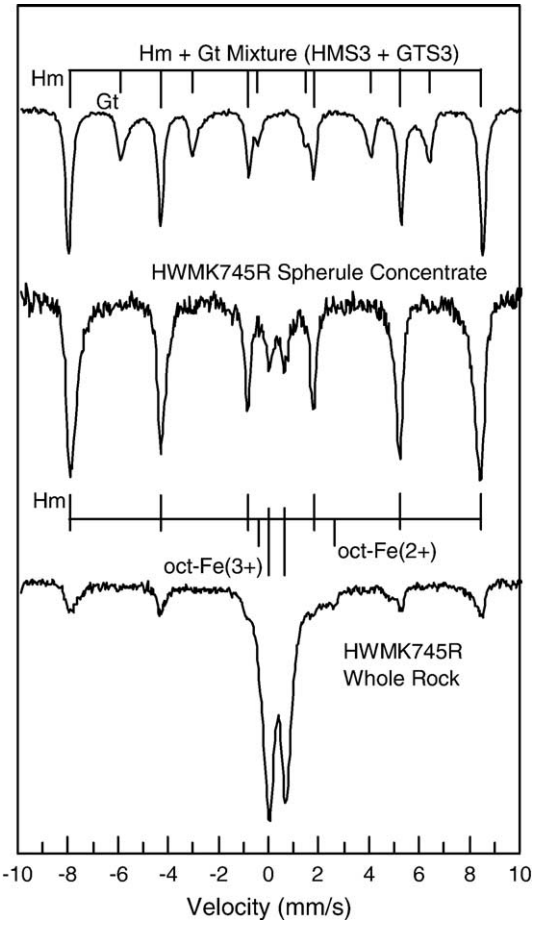

Fig. 3. Mössbauer spectra (293 K) for a mechanical mixture of synthetic and well-crystalline hematite (HMS3) and goethite (GTS3), a spherule concentrate from HWMK745R, and whole rock HWMK745R. The spectrum of the spherule concentrate is interpreted by a hematite sextet with no detectable goethite sextet plus a doublet from whole-rock contamination in the concentrate.

Table 2
Mössbauer parameters (295 K) for HWMK745R spherule concentrate and whole rock and a hematite+goethite mechanical mixture

	δ (mm/s)	ΔE_Q (mm/s)	B_{hf} (T)	A^a (%)
HWMK745R spherule concentrate				
Hematite sextet	0.37	−0.20	51.0	88
Fe^{3+} doublet	0.34	0.61	–	12
HWMK745 whole rock				
Hematite sextet	0.37	−0.18	50.6	22
Fe^{3+} doublet	0.36	0.69	–	72
Fe^{2+} doublet	1.09	2.81	–	6
HMS3+GTS3 mixture				
Hematite	0.37	−0.21	51.4	65
Goethite	0.37	−0.26	38.6	35
Uncertainty	±0.02	±0.02	±0.4	±2

[a] Relative subspectrum area includes *f*-factor correction $f(Fe^{3+})/f(Fe^{2+})=1.21$.

values are within error of the values reported in the literature for hematite [21–23]. The asymmetric line shapes imply a distribution of magnetic hyperfine fields that is skewed toward lower values. In MK spherules, we attribute the skewed distribution to both Al^{3+} for Fe^{3+} substitution in hematite [24] as indicated by the elemental analyses and to the presence of H_2O/OH^{-1} in the hematite structure [20] as indicated by the low element totals.

4. Whole rock

The whole rock Mössbauer spectrum of HWMK-745R is characterized (Fig. 3; Table 2) by doublets from octahedrally coordinated Fe^{3+} (oct-Fe^{3+}; 72%), oct-Fe^{2+} (6%), and a hematite sextet (22%). The mineralogical assignment of the doublets in this complex rock is not possible with current information. EDS analyses indicate that there are regions rich in Al, S, Na, and Fe (Fe-rich natroalunite?), suggesting contributions to the Fe^{3+} doublet from this source. Also possible is Fe^{3+} in smectite. Although hematite is a substantial component in the whole-rock Mössbauer spectrum of HWMK745R (Fig. 3), the whole rock XRD powder pattern (Fig. 4) is dominated by peaks from plagioclase feldspar, natroalunite, and smectite. A low-intensity peak at the position corresponding to the most intense peak in the XRD pattern for well-crystalline hematite is indicated by the arrow. EMP analyses of particles other than spherules in the polished grain mount of the spherule concentrate and mineral grains in the polished thick section (Table 3) show that plagioclase feldspar, olivine, and Fe–Ti oxide are present. Either these primary mineral phases were protected from alteration by the sulfate-rich aqueous fluids or the reaction kinetics were slow relative to the timescale of the alteration event(s). We attempted analyses on the S-rich rock surrounding the spherules in the thick section, but severe damage by the electron beam occurred, making the analyses unreliable (totals 106–125%).

Element X-ray maps for a spherule and surrounding S-rich matrix in a polished thick section (Fig. 5) show elongated areas in the matrix (black arrows) where the enrichments of S, Al, Ca, and P are strongly correlated. Mg also weakly correlates with these elements, but the association is not so obvious. The Si map shows Si depletion in the areas where S, Al, Ca, and P show enrichment. Mn is highly correlated with the Fe-rich

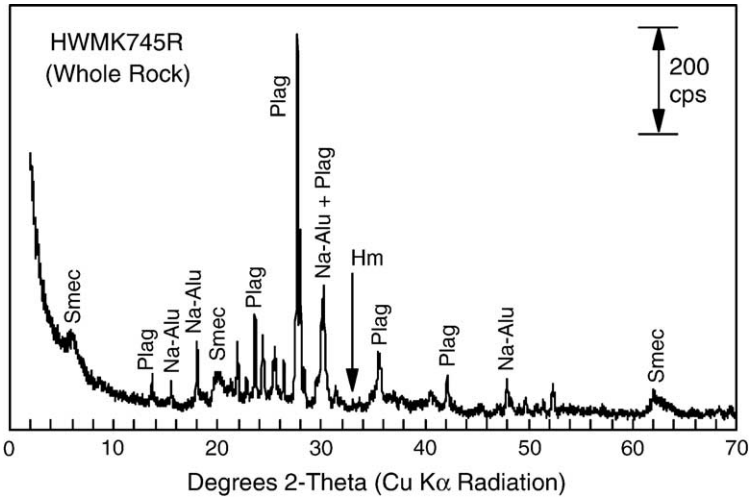

Fig. 4. Powder X-ray diffraction pattern for whole-rock HWMK745R. The major peaks are from plagioclase feldspar (Plag), natroalunite (Na-Alu), and smectite (Smec). Arrow indicates the most intense peak for hematite (Hm).

Table 3
Electron microprobe analyses of mineral grains from HWMK745R (concentrations in wt. %)

Phase	Feldspar		Olivine		Pyroxene	Fe–Ti oxide	
analysis	1	2	3	4	5	6	7
SiO_2	55.24	53.99	38.12	36.66	51.09	0.49	0.21
TiO_2	0.16	0.11	0.05	0.17	0.93	17.35	16.66
Al_2O_3	27.48	28.32	0.05	0.12	2.25	6.13	6.60
Cr_2O_3	0.00	0.02	0.00	0.04	0.40	0.05	0.01
Fe_2O_3T[a]	1.74	0.50	0.00	0.00	9.06	70.71	69.68
FeOT[a]	0.00	0.00	26.27	31.15	0.00	0.00	0.00
MnO	0.02	0.03	0.56	0.69	0.17	0.08	0.00
MgO	0.08	0.05	35.86	29.53	16.66	4.93	5.14
CaO	9.53	10.67	0.24	0.29	19.94	0.01	0.02
Na_2O	4.79	4.74	0.00	0.02	0.25	0.01	0.03
K_2O	0.53	0.32	0.00	0.02	0.01	0.00	0.00
P_2O_5	0.12	0.17	0.09	0.39	0.21	0.00	0.00
SO_3	0.03	0.03	0.02	0.01	0.00	0.05	0.04
CoO	0.00	nd	0.00	0.00	0.01	0.00	nd
NiO	0.00	nd	0.02	0.04	0.03	0.00	nd
Total	99.73	98.95	101.28	99.13	101.01	99.82	98.39

[a] Total Fe expressed as Fe_2O_3 or FeO.

spherule, perhaps in solid solution as the $MnFe_2O_4$ molecule. Si and especially Ti are enriched in the region immediately surrounding the spherule.

Differences in major element compositions between whole-rock HWMK745R and its hawaiite–meugerite precursor (Table 4) are significant on a volatile-free basis. Consistent with the presence of hematite, natroalunite, and smectite, HWMK745R is oxidized ($Fe^{3+}/Fe_T = 0.98$) and volatile rich (LOI = 18.76%). Relative to its precursor, the breccia is strongly enriched in Al and P and strongly depleted in Si, Mg, and Mn. Mg and Mn are the two most depleted elements in the sulfate-rich tephra samples from Mauna Kea studied by [19]. Elemental differences are not explained by the simple addition (e.g., natroalunite) or subtraction (e.g., silica) of any single component. Presumably, the observed elemental composition is a result of a complex alteration history involving the aqueous alteration of glassy tephra at near neutral pH before the onset of acid-sulfate alteration, the aqueous acid-sulfate alteration itself, and the subsequent leaching of soluble components by near neutral water (from rain and snow) under ambient conditions after acid-sulfate alteration of Puu Poliahu ceased.

A consistent but not unique qualitative explanation of the whole-rock elemental and mineralogical compositions is isochemical alteration of glassy precursor tephra by one or more episodes of aqueous alteration by acid-sulfate solutions to opaline silica, smectite, hematite, and sulfates including natroalunite, jarosite, and Mg-rich sulfates. At least some of the primary minerals (e.g., plagioclase and olivine) resisted or were protected from alteration. The relatively sharp transition from Fe-rich core to more Al-rich rim for the hematite spherules implies a change in environmental conditions and/or a change in composition of aqueous fluids. After cessa-

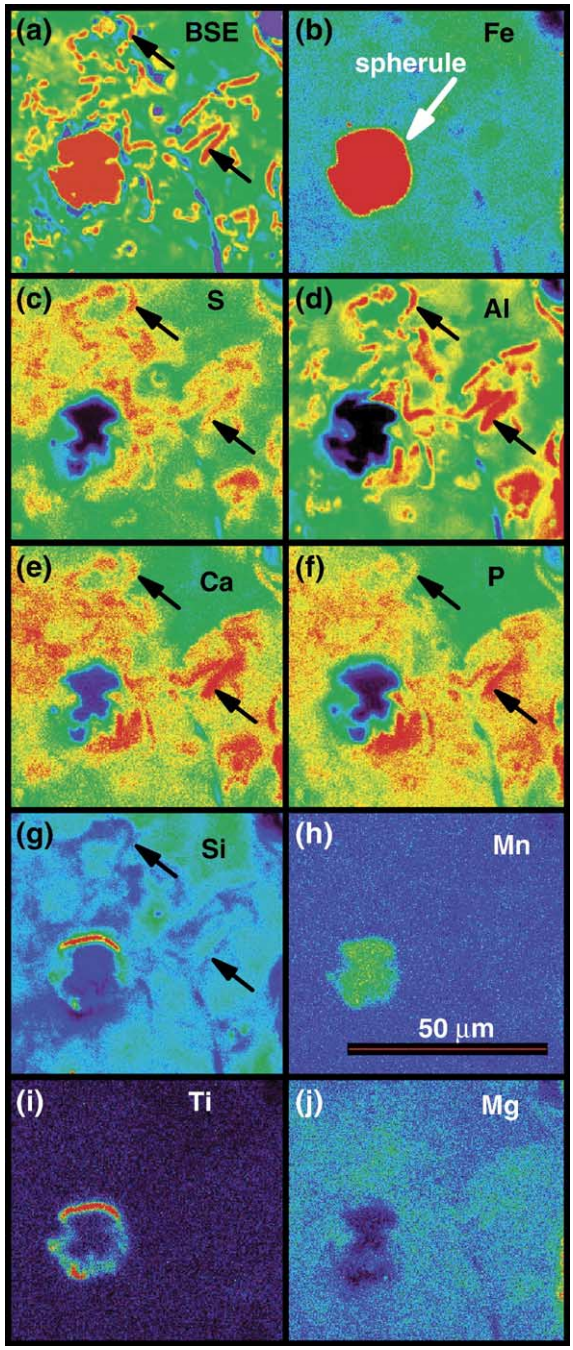

Fig. 5. Major element maps for a hematite spherule imbedded in a S-bearing matrix. Black arrows indicate elongated regions enriched in S, Al, Ca, and P and depleted in Si. Red=high; black=low.

Table 4
XRF analyses of whole rock HWMK745R and unaltered precursor (concentrations in wt. %)

	HWMK745R	Unaltered[a]
SiO_2	43.59	49.74
TiO_2	2.14	2.77
Al_2O_3	28.02	17.37
Cr_2O_3	0.01	0.00
Fe_2O_3T	12.21	12.03
MnO	0.07	0.21
MgO	0.98	3.93
CaO	5.09	6.60
Na_2O	3.87	4.33
K_2O	2.21	1.90
P_2O_5	1.64	0.85
SO_3	nd	0.09
Total	100.19	99.83
% LOI[b]	18.76	1.60
FeO	0.27	6.02
Fe_2O_3	11.91	5.34

[a] From Morris et al. [19].
[b] LOI = Weight loss on ignition after heating to 950 °C in air for 1 h.

tion of aqueous, acid-sulfate alteration, the soluble Mg-rich sulfates and some opaline silica were removed by aqueous leaching (rain and snow water) under approximately neutral pH conditions, giving the observed depletions in Mg and Si. An alternative is that these elements were carried away by the acid-sulfate fluids.

5. Mauna Kea hematite spherule formation process

Independent of considerations relating to spherule morphology, the observational evidence is that hematite in breccia HWMK745R formed by aqueous precipitation under acid-sulfate conditions in basaltic terrain. This result is based on field observations, the basaltic bulk elemental composition of unaltered tephra samples, and mineralogical analyses of HWMK745R and other rocks from the same area on Mauna Kea that establish the presence of sulfate minerals like natroalunite and jarosite. The apparent absence of hematite spherules in areas on Mauna Kea where aqueous alteration has taken place without formation of sulfate minerals [19] implies that acid-sulfate conditions are necessary for their formation. The origin of the spheroidal shape is less constrained.

In laboratory experiments, hematite particles can be precipitated from aqueous solutions with narrow size distributions and specific morphologic forms during forced hydrolysis at ~100 °C by the presence of additives and/or the alteration of reaction conditions [e.g., 25,26]. For example, the presence of chloride in acidic solutions can promote the formation of spherical hematite particles in the size range ~0.05–0.5 μm. Although forced hydrolysis of Fe-bearing solutions would occur under natural hydrothermal conditions, the experimental evidence just cited does not seem consistent with precipitation of spherical hematite particles on Mauna Kea, because the presence of sulfates like natroalunite and jarosite implies aqueous fluids that are dominated by sulfate and not chloride anions. The diameter of MK spherules is also a factor of ~200 larger than spherules produced in laboratory experiments. However, forced hydrolysis employing solutions simulating realistic aqueous fluids has not been investigated in laboratory experiments, and, in any case, time-scales required for the process to produce large spherules may be possible only in natural geologic environments. It is possible, for example, that the Al^{3+} cation, because it is incorporated in the MK spherules, promotes the formation of hematite spherules during forced hydrolysis of Fe-rich acid-sulfate solutions.

6. Application to the Meridiani Planum outcrop

The grey (i.e., spectrally neutral at visible wavelengths) hematite spherules observed on Mauna Kea volcano are mineralogically and morphologically similar to the spherules detected in the sulfate-rich outcrop at Meridiani Planum (the Burns formation). In both locations, individual and interlocking spherules are present (Fig. 2c and [9]). Both occurrences are associated with sulfate-bearing minerals (natroalunite and jarosite for Mauna Kea and jarosite and Ca–Mg sulfates for Meridiani Planum [5,12]), and both are associated with terrain that has a basaltic bulk composition (Table 1 and [13]).

The Meridiani spherules within the outcrop are about two orders of magnitude larger than MK spherules (~100 μm). As noted earlier, a second population of hematite particles is present in the sulfate-rich rock that surrounds the MP spherules, according to MB measurements [12]. Because distinct carriers of this hematite are not obvious in MI images, the particle diameter is probably too small to be detectable using the 30 ìm/pixel resolution of the MI [27]. The largest MK spherules are also too small to be detected at MI resolution. Therefore, the possibility is open that hematite spherules comparable in diameter (and composition) to those on Mauna Kea are present but not imaged in the sulfate-rich rock that surrounds the larger MP spherules.

There are other differences between MK and MP spherules and the terrains in which they occur. Al-

though the MK spherules are mineralogically hematite according to MB, they exhibit concentric zoning with respect to elemental composition (Table 1 and Fig. 2). The manifestation of this symmetry in reflected visible light is a change in albedo. Variations in albedo are not apparent in MI and Pancam images of MP spherules that have been sectioned by the MER RAT [7,10], providing no evidence for compositional heterogeneity. Freshly broken MK spherules have a radial texture, but this texture is not observed in broken MP spherules, although it could be erased by wind-driven sand blasting of the broken spherule surfaces. The radial texture is not observed in sectioned spherules from both locations. The areal extent of alteration of basaltic material on Mauna Kea is very small in comparison to the Meridiani Planum outcrop (~1 km^2 compared to ~3×10^5 km^2 [2]). Finally, the elemental composition of sulfate-rich material on Mauna Kea is highly variable compared to the analyzed regions of Meridiani Planum outcrop [13,19].

What are the implications of these similarities and differences for the mineralogy, composition, and formation pathway for outcrop hematite, both within the spherules and, perhaps, within the sulfate-rich rock surrounding the spherules? First, the Mauna Kea occurrence documents that it is possible, with basaltic precursor material, to produce hematite spherules during aqueous, acid-sulfate alteration. We do not know, with available data, if the MK spherules formed directly from basaltic material in one aqueous event (dissolution of basaltic material and precipitation of hematite spherules) or whether multiple events occurred. A two step process could involve formation of sulfates and other alteration products in the first step and dissolution of sulfates and other materials to form hematite concretions by hydrolysis in the second step. The two-step process is consistent with the model of [11] for the MP spherules where they are rapidly formed by a distinct groundwater event that hydrolyzes pre-existing jarosite and other sulfate rocks and precipitates hematite concretions. Rapid hydrolysis under hydrothermal conditions is implicated for the MK spherule occurrence, but such conditions may not be a requirement for MP spherules if the time interval for hydrolysis at lower temperatures is sufficiently long. The apparent absence of elemental zoning in the Meridiani spherules may imply that environmental conditions and compositions of acid-sulfate solutions were more constant during formation of the MP spherules than for the MK spherules.

The presence of two hematite populations in the Meridiani Planum outcrop implies more than one hematite-forming process or episode. The large MP spherules could have formed rapidly during a relatively discrete event as proposed by [11]. The hematite within the sulfate-rich rock may (a) have formed during a second discrete event whose defining parameters produced only small hematite particles (<100 μm in diameter), (b) be continuously produced by very slow hydrolysis of Fe-sulfates (e.g., jarosite), or (c) have formed prior to the large MP spherules when the sulfate-rich rock was initially deposited. By analogy with MK spherules and synthetic hematite produced by forced hydrolysis, the MP spherules and hematite within the sulfate-rich rock may be solid solutions of hydrohematite, protohematite, and hematite and thus could contribute to the water inventory at Meridiani Planum.

Acknowledgements

We acknowledge the insightful, pioneering, and persistent advocacy of our late colleague Dr. Roger G. Burns for sulfates on Mars. This research was funded by the NASA Mars Fundamental Research Program, the NASA Mars Exploration Rover Project, the NASA Mars Reconnaissance Orbitor Project, and the NASA Planetary Geology and Geophysics Program. We thank Scott McLennan, Wayne Hudnall, and Wendy Gagliano for thoughtful reviews of the manuscript.

References

[1] P.R. Christensen, J.L. Bandfield, R.N. Clark, K.S. Edgett, V.E. Hamilton, T. Hoefen, H.H. Kieffer, R.O. Kuzmin, M.D. Lane, M.C. Malin, R.V. Morris, J.C. Pearl, R. Pearson, T.L. Roush, S.W. Ruff, M.D. Smith, Detection of crystalline hematite mineralization on Mars by the thermal emission spectrometer, J. Geophys. Res. 105 (2000) 9623–9642.

[2] P.R. Christensen, R.V. Morris, M.D. Lane, J.L. Bandfield, M.C. Malin, Global mapping of martian hematite mineral deposits: remnants of water-driven processes on early Mars, J. Geophys. Res. 106 (2001) 23,873–23,885.

[3] R.E. Arvidson, R.C. Anderson, A.F.C. Haldemann, G.A. Landis, R. Li, R.A. Lindemann, J.R. Matijevic, R.V. Morris, L. Richter, S.W. Squyres, R.J. Sullivan, N.O. Snider, Physical properties and localization investigations associated with the 2003 Mars exploration rovers, J. Geophys. Res. 108 (2003) 8070, doi:10.1029/2002JE002041.

[4] M.P. Golombek, J.A. Grant, T.J. Parker, D.M. Kass, J.A. Crisp, S.W. Squyres, A.F.C. Haldemann, M. Adler, W.J. Lee, N.T. Bridges, R.E. Arvidson, M.H. Carr, R.L. Kirk, P.C. Knocke, R.B. Roncoli, C.M. Weitz, J.T. Schofield, R.W. Zurek, P.R. Christensen, R.L. Fergason, F.S. Anderson, J.W. Rice Jr., Selection of the Mars exploration rover landing sites, J. Geophys. Res. 108 (2003) 8072, doi:10.1029/2003JE002074.

[5] P.R. Christensen, M.B. Wyatt, T.D. Glotch, A.D. Rogers, S. Anwar, R.E. Arvidson, J.L. Bandfield, D.L. Blaney, C. Budney, W.M. Calvin, A. Fallacaro, R.L. Fergason, N. Gorelick, T.G.

Graff, V.E. Hamilton, A.G. Hayes, J.R. Johnson, A.T. Knudson, H.Y. McSween Jr., L.K. Mehall, J.E. Moersch, R.V. Morris, M.D. Smith, S.W. Squyres, S.W. Ruff, M.J. Wolff, Mineralogy at Meridiani Planum form the mini-TES experiment on the Opportunity rover, Science 306 (2004) 1733–1739.

[6] J.F. Bell III, S.W. Squyres, R.E. Arvidson, H.M. Arneson, D. Bass, W. Calvin, W.H. Farrand, W. Goetz, M. Golombek, R. Greeley, J. Grotzinger, E. Guinness, A.G. Hayes, M.Y.H. Hubbard, K.E. Herkenhoff, M.J. Johnson, J.R. Johnson, J. Joseph, K.M. Kinch, M.T. Lemmon, R. Li, M.B. Madsen, J.N. Maki, M. Malin, E. McCartney, S. McLennan, H.Y. McSween, D.W. Ming, R.V. Morris, E.Z. Noe Dobrea, T.J. Parker, J. Proton, J.W. Rice, F. Seelos, J.M. Soderblom, L.A. Soderblom, J.N. Sohl-Dickstein, R.J. Sullivan, M.J. Wolff, A. Wang, Pancam multispectral imaging results from the opportunity rover at Meridiani Planum, Science 306 (2004) 1703–1709.

[7] L.A. Soderblom, R.C. Anderson, R.E. Arvidson, J.F. Bell III, N.A. Cabrol, W. Calvin, P.R. Christensen, B.C. Clark, T. Economou, B.L. Ehlmann, W.F. Farrand, D. Fike, R. Gellert, T.D. Glotch, M.P. Golombek, R. Greeley, J.P. Grotzinger, K.E. Herkenhoff, D.J. Jerolmack, J.R. Johnson, B. Jolliff, G. Klingelhoefer, A.H. Knoll, Z.A. Learner, R. Li, M.C. Malin, S.M. McLennan, H.Y. McSween, D.W. Ming, R.V. Morris, J.W. Rice Jr., L. Richter, R. Rieder, D. Rodionov, C. Schroeder, F.P. Seelos IV, J.M. Soderblom, S.W. Squyres, R. Sullivan, W.A. Watters, C.M. Weitz, M.B. Wyatt, A. Yen, J. Zipfel, Soils of eagle crater and Meridiani Planum at the Opportunity Rover landing site, Science 306 (2004) 1723–1726.

[8] R.E. Arvidson, R.C. Anderson, P. Bartlett, J.F. Bell III, P.R. Christensen, P. Chu, K. Davis, B.L. Ehlmann, M.P. Golombek, S. Gorevan, E.A. Guinness, A.F.C. Haldemann, K.E. Herkenhoff, G. Landis, R. Li, R. Lindemann, D.W. Ming, T. Myrick, T. Parker, L. Richter, F.P. Seelos IV, L.A. Soderblom, S.W. Squyres, R.J. Sullivan, J. Wilson, Localization and physical property experiments conducted by opportunity at Meridiani Planum, Science 306 (2004) 1723–1726.

[9] K.E. Herkenhoff, S.W. Squyres, R. Arvidson, D.S. Bass, J.F. Bell III, P. Bertelsen, B.L. Ehlmann, W. Farrand, L. Gaddis, R. Greeley, J. Grotzinger, A.G. Hayes, S.F. Hviid, J.R. Johnson, B. Jolliff, K.M. Kinch, A.H. Knoll, M.B. Madsen, J.N. Maki, S.M. McLennan, H.Y. McSween, D.W. Ming, J.W. Rice Jr., L. Richter, M. Sims, P.H. Smith, L.A. Soderblom, N. Spanovich, R. Sullivan, S. Thompson, T. Wdowiak, C. Weitz, P. Whelley, Evidence from Opportunity's Microscopic Imager for water on Meridiani Planum, Science 306 (2004) 1723–1726.

[10] S.W. Squyres, J.P. Grotzinger, R.E. Arvidson, J.F. Bell III, W. Calvin, P.R. Christensen, B.C. Clark, J.A. Crisp, W.H. Farrand, K.E. Herkenhoff, J.R. Johnson, G. Klingelhoefer, A.H. Knoll, S.M. McLennan, H.Y. McSween Jr., R.V. Morris, J.W. Rice Jr., R. Rieder, L.A. Soderblom, In situ evidence for an ancient aqueous environment at Meridiani Planum, Mars, Science 306 (2004) 1731–1733.

[11] S.M. McLennan, J.F. Bell III, W.M. Calvin, P.R. Christensen, B.C. Clark, P.A. de Souza, J. Farmer, W. H. Farrand, D. A. Fike, R. Gellert, A. Ghosh, T. D. Glotch, J.P. Grotzinger, B. Hahn, K.E. Herkenhoff, J.A. Hurowitz, J.R. Johnson, S.S. Johnson, B. Jolliff, G. Klingelhöfer, A. H. Knoll, Z. Learner, M.C. Malin, H.Y., McSween Jr., J. Pocock, S.W. Ruff, L. A. Soderblom, S.W. Squyres, N.J. Tosca, W.A. Watters, M.B. Wyatt, A. Yen, Provenance and diagenesis of the Burns formation, Meridiani Planum, Mars, Earth Planet. Sci. Lett. 240 (2005) 95–121, doi:10.1016/j.epsl.2005.09.041.

[12] G. Klingelhoefer, R.V. Morris, B. Bernhardt, C. Schroeder, D.S. Rodionov, P.A. de Souza Jr., A. Yen, R. Gellert, E.N. Evlanov, B. Zubkov, J. Foh, U. Bonnes, E. Kankeleit, P. Gutlich, D.W. Ming, F. Renz, T. Wdowiak, S.W. Squyres, R.E. Arvidson, Jarosite and hematite at Meridiani Planum from opportunity's Mössbauer spectrometer, Science 306 (2004) 1740–1745.

[13] R. Rieder, R. Gellert, R.C. Anderson, J. Breuchner, B.C. Clark, G. Dreibus, T. Economou, G. Klingelhoefer, G.W. Lugmair, D.W. Ming, C. d'Uston, H. Waenke, A. Yen, J. Zipfel, Chemistry of rocks and soils at Meridiani Planum from the alpha particle X-ray spectrometer, Science 306 (2004) 1746–1749.

[14] M.A. Chan, B. Beitler, W.T. Parry, J. Ormo, G. Komatsu, A possible terrestrial analogue for haematite concretions on Mars, Nature 429 (2004) 731–734.

[15] E.W. Wolfe, W.S. Wise, G.B. Dalrymple, The Geology and Petrology of Mauna Kea Volcano, Hawaii: A Study of Postshield Volcanism, in: U.S. Geological Survey Prof Paper, vol. 1557, U.S.Government Printing Office, Washington, 1997.

[16] F.C. Ugolini, Hydrothermal origin of the clays from the upper slopes of Mauna Kea, Hawaii, Clays Clay Miner. 22 (1974) 189–194.

[17] D.C. Golden, R.V. Morris, D.W. Ming, H.V. Lauer Jr., S.R. Yang, Mineralogy of three slightly palagonitized tephra samples from the summit of Mauna Kea Hawaii, J. Geophys. Res. 98 (1993) 3401–3411.

[18] R.V. Morris, D.W. Ming, D.C. Golden, J.F. Bell III. An occurrence of jarositic tephra on Mauna Kea, Hawaii: Implications for the ferric mineralogy of the martian surface, in Mineral Spectroscopy: A Tribute to Roger G. Burns, M.D. Dyar, C. McCammon, and M.W. Schaefer (Eds.), The Geochemical Society, Special Publication No. 5, Houston (1996) 327–336.

[19] R.V. Morris, D.C. Golden, J.F. Bell III, T.D. Shelfer, A.C. Scheinost, N.W. Hinman, G. Furniss, S.A. Mertzman, J.L. Bishop, D.W. Ming, C.C. Allen, D.T. Britt, Mineralogy, composition, and alteration of Mars Pathfinder rocks and soils: evidence from multispectral, elemental, and magnetic data on terrestrial analogue, SNC meteorite, and pathfinder samples, J. Geophys. Res. 105 (2000) 1757–1817.

[20] M.-Z. Dang, D.G. Rancourt, J.E. Dutrizac, G. Lamarche, R. Provencher, Interplay of surface conditions, particle size, stoichiometry, cell parameters, and magnetism in synthetic hematite-like minerals, Hyperfine Interact. 117 (1998) 271–319.

[21] R.V. Morris, H.V. Lauer Jr., C.A. Lawson, E.K. Gibson Jr., G.A. Nace, C. Stewart, Spectral and other physicochemical properties of submicron powders of hematite (α-Fe_2O_3), maghemite (γ-Fe_2O_3), magnetite (Fe_3O_4), goethite (α-FeOOH), and lepidocrocite (γ-FeOOH), J. Geophys. Res. 90 (1985) 3126–3144.

[22] J.G. Stevens, A.M. Khasanov, J.W. Miller, H. Pollak, Z. Li, Mössbauer Mineral Handbook, Biltmore Press, Ashville, NC, 1998.

[23] C. McCammon, Mössbauer spectroscopy of minerals, in: T.J. Ahrens (Ed.), Mineral Physics and Crystallography: A Handbook of Physical Constants, American Geophysical Union, Washington DC, 1995, pp. 332–347.

[24] E. Murad, U. Schwertmann, Influence of Al substitution and crystal size on the room-temperature Mössbauer spectrum of hematite, Clays Clay Miner. 34 (1986) 1–6.

[25] E. Matijevic, P. Scheiner, Ferric hydrous oxide sols III. Preparation of uniform particles by hydrolysis of Fe(III)-chloride, -nitrate, and -perchlorate solutions, J. Colloids Interface Sci. 63 (1978) 509–524.

[26] K. Kandori, J. Sakai, T. Ishikawa, Definitive effects of chloride ions on the formation of spherical hematite particles in a forced hydrolysis reaction, Phys. Chem. Chem. Phys. 2 (2000) 3293–3299.
[27] K.E. Herkenhoff, S.W. Squyres, J.F. Bell III, J.N. Maki, H.M. Arneson, P. Bertelsen, D.I. Brown, S.A. Collins, A. Dingizian, S.T. Elliott, W. Goetz, E.C. Hagerott, A.G. Hayes, M.J. Johnson, R.L. Kirk, S. McLennan, R.V. Morris, L.M. Scherr, M.A. Schwochert, L.R. Shiraishi, G.H. Smith, L.A. Soderblom, J.N. Sohl-Dickstein, M.V. Wadsworth, Athena microscopic imager investigation, J. Geophys. Res. 108 (2003) 8065, doi:10.1029/2003JE002076.